Annu. Rev. Fluid Mech. 2003. 35:89–111
doi: 10.1146/annurev.fluid.35.101101.161102


# AERODYNAMICS OF SMALL VEHICLES

Thomas J. Mueller[1] and James D. DeLaurier[2]
[1]*Hessert Center for Aerospace Research, Department of Aerospace and Mechanical Engineering, University of Notre Dame, Notre Dame, Indiana 46556; email: mueller.1@nd.edu,*
[2]*Institute for Aerospace Studies, University of Toronto, Downsview, Ontario, Canada M3H 5T6; email: jdd@utias.utoronto.ca*



**Key Words** low Reynolds number, fixed wing, flapping wing, small unmanned vehicles

■ **Abstract** In this review we describe the aerodynamic problems that must be addressed in order to design a successful small aerial vehicle. The effects of Reynolds number and aspect ratio (AR) on the design and performance of fixed-wing vehicles are described. The boundary-layer behavior on airfoils is especially important in the design of vehicles in this flight regime. The results of a number of experimental boundary-layer studies, including the influence of laminar separation bubbles, are discussed. Several examples of small unmanned aerial vehicles (UAVs) in this regime are described. Also, a brief survey of analytical models for oscillating and flapping-wing propulsion is presented. These range from the earliest examples where quasi-steady, attached flow is assumed, to those that account for the unsteady shed vortex wake as well as flow separation and aeroelastic behavior of a flapping wing. Experiments that complemented the analysis and led to the design of a successful ornithopter are also described.

## 1. INTRODUCTION

Interest in the design and development of small unmanned aerial vehicles (UAVs) has increased dramatically in the past two and a half decades. These vehicles can perform a large variety of missions including surveillance, communication relay links, ship decoys, and detection of biological, chemical, or nuclear materials. These missions are ideally suited to small UAVs that are either remotely piloted or autonomous. Requirements for a typical low-altitude small UAV include long flight duration at speeds between 20 and 100 km/h (12 to 62 mile/h), cruise altitudes of 3 to 300 m (10 to 1000 ft), light weight, and all-weather capabilities. Although the definition of small UAVs is somewhat arbitrary, vehicles with wing spans less than approximately 6 m (20 ft) and masses less than ∼25 kg (55 lb) are usually considered in this category. Because of the recent availability of very small sensors, video cameras, and control hardware, systems as small as 15 cm (6 in) with a mass of 80 g (2.8 oz), referred to as micro-air vehicles (MAVs), are now possible for limited missions.

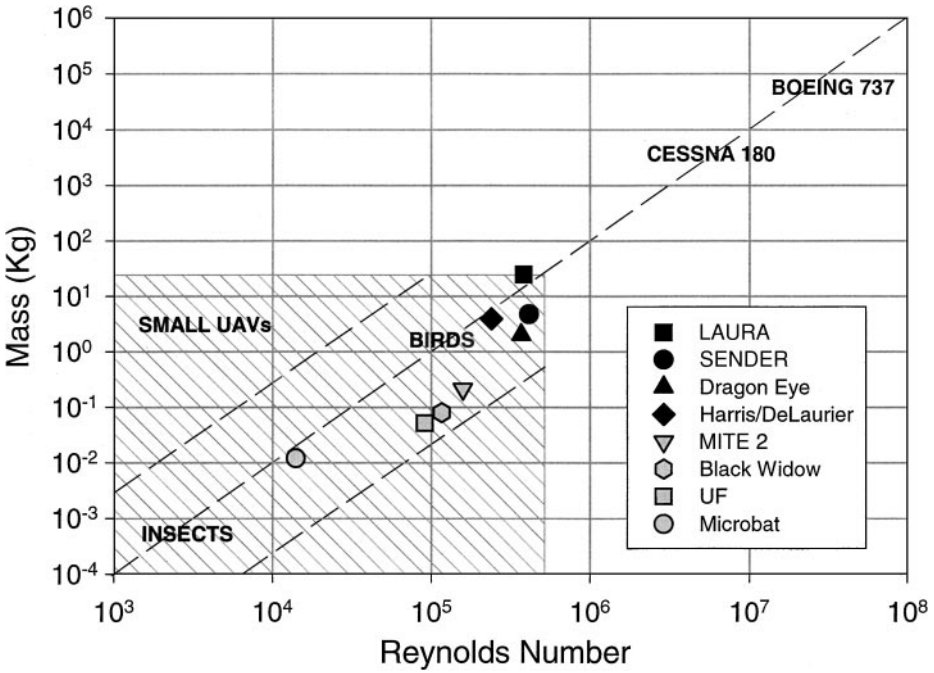


**Figure 1** Reynolds number range for flight vehicles.

The combination of small length scale and low velocities results in a flight regime with low-wing chord Reynolds numbers (i.e., chord Reynolds numbers ranging from ∼15,000 to 500,000). The nondimensional chord Reynolds number is defined as the cruise speed times the mean wing chord divided by kinematic viscosity of air. Figure 1 shows the relationship between total mass and wing chord Reynolds number for various flight vehicles. The small UAV regime, which includes MAVs, is well below that of conventional aircraft. These small UAVs are actually in a regime occupied by birds and model airplanes. These vehicles require efficient low Reynolds number airfoils that are not overly sensitive to wind shear, gusts, and the roughness produced by precipitation. Minimum wing area for ease of packaging and prelaunch handling is also important.

Although it is desirable for small UAVs to be able to fly when large wind gusts are present, there are no published studies that address this problem. In fact, quantitative studies of unsteady aerodynamics directly related to small UAVs, with the exception of flapping-wing vehicles, at low Reynolds numbers have only recently become of interest (e.g., Broeren & Bragg 2001). In some cases, wind-tunnel studies are made but not published for proprietary reasons. There are, however, a number of studies of the steady aerodynamics of airfoils that are very useful in the design of small fixed-wing UAVs. The U.S. Naval Research Laboratory (NRL)

has been a leader in the design of small fixed-wing UAVs, and most of the vehicles mentioned here are from their published results. There are also a number of studies of the unsteady aerodynamics related to flapping-wing UAVs. The following sections include a description of several successful fixed- and flapping-wing vehicles as well as the fluid-dynamic problems related to the design and performance of these vehicles.

## 2. SMALL UAV AND MAV EXAMPLES

The mass versus wingspan of the small and MAVs of Figure 1 is shown in Figure 2. Both fixed- and flapping-wing vehicles are included in this figure. Although there are many other vehicles in this regime, it is difficult to find references that include detailed information. The largest of these vehicles are the LAURA vehicles, which were designed for long endurance as active ship decoys (see Cross 1989, Evangelista et al. 1989, Foch & Toot 1989, Siddiqui et al. 1989, Foch & Ailinger 1992). All four of the LAURA configurations shown in Figure 3 had a common fuselage, payload, landing gear, and propulsion system. The propulsion system consisted of a reciprocating engine and pusher propeller on the aft end of

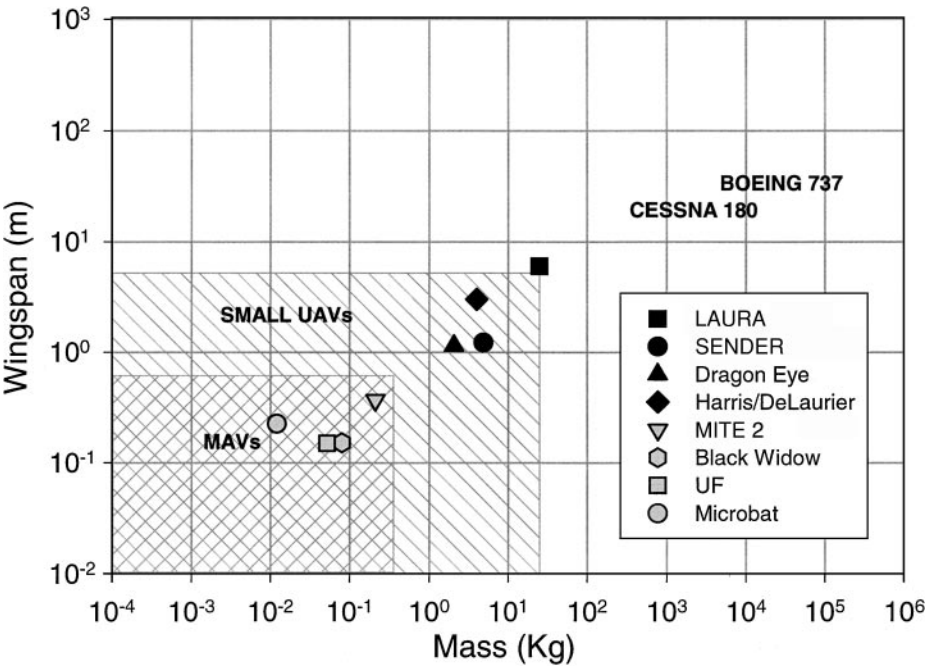


**Figure 2** Wingspan versus mass for small UAVs and MAVs.

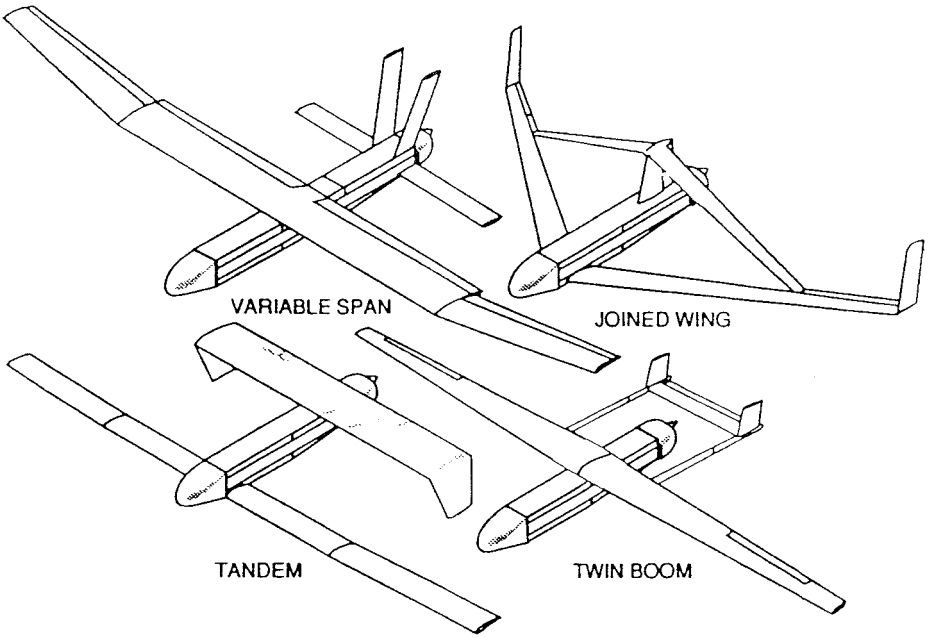


**Figure 3** Sketch of the four LAURA vehicles.



the fuselage. These were experimental vehicles and were designed to study various wing configurations and low Reynolds number airfoil sections.

The SENDER, shown in Figure 4, used the Selig SD7032 airfoil and was designed to be a fully autonomous vehicle with global-positioning system (GPS) navigation, to have a man-in-the-loop option, and to be a one-man portable UAV. This electrically powered vehicle was also designed to fit into a standard suitcase, to carry a wide variety of payloads, and to cruise at ~91 km/h (56 mph) for up to 2 h (Foch 1996). This vehicle flew successfully; however, the complete supporting system was not developed.

The Dragon Eye airborne sensor system shown in Figure 4 has several unique features. This small UAV can be assembled and disassembled without any tools and can be stored in a container with the dimensions $18 \times 38 \times 38$ cm ($7 \times 15 \times 15$ in), which can be carried as a backpack (Foch et al. 2000). This vehicle features autonomous flight with one-person operation and GPS navigation. It is electrically powered and can fly for 30 to 60 min at 64 km/h (40 mph). The Dragon Eye can use interchangeable off-the-shelf payloads that include daylight, low-light, and infrared imaging systems and robust communication links. It is currently being manufactured by AeroVironment, Inc. and BAI Aerosystems.

The MITE 2, shown in Figure 4, has a wing span of 36 cm (14.5 in) and is one of a series of MAV research vehicles designed to be an affordable, expendable covert sensor platform for close-in short-duration missions (see Kellogg et al. 2001a).

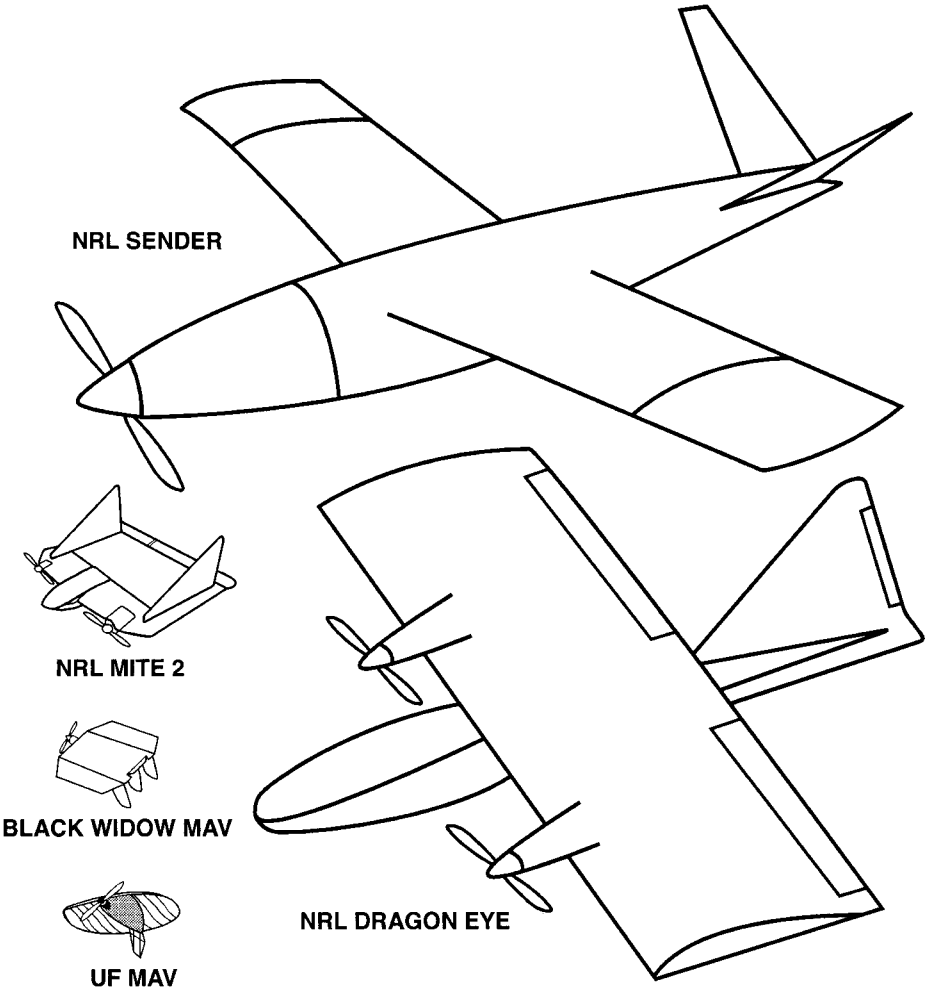


**Figure 4** Sketch of recent, small fixed-wing UAVs (SENDER, Dragon Eye, MITE 2, and Black Widow).

It is an electrically powered, twin-motor vehicle that can carry a useful military payload at 32 km/h (20 mph) for 20 min.

One of the smallest MAVs that can carry a useful payload is the Black Widow developed by AeroVironment, Inc. (Grasmeyer & Keennon 2001). This vehicle (see Figure 4) is electrically powered, has a maximum dimension of 15.2 cm (6 in) and a total mass of ∼80 g (2.8 oz), and can carry a color video camera and transmitter at 51 km/h (32 mph) for 30 min. The Black Widow is transported in a 6.8-kg (15-lb) briefcase that also contains a pneumatic launcher and a removable pilot's control unit with a 10-cm (4 in) liquid-crystal display.

The University of Florida has developed a flexible-wing concept and applied it to MAV design (see Shyy et al. 1999, Levin & Shyy 2001, Ifju et al. 2002). The smallest vehicle is powered by a reciprocating engine, has a maximum dimension of 15.2 cm (6 in) and a total mass of 52 g (1.8 oz), and flies at speeds of between 24 and 40 km/h (15 and 25 mph, respectively) for ∼15 min while carrying a video camera and transmitter (see Figure 4). Flight tests on 25.4-cm (10-in) vehicles with either flexible or rigid wings indicate that the flexible wings offer measurable stability and ease-of-control advantages (Ifju et al. 2002).

The recent interest in small UAVs and MAVs has focused attention on mechanical flapping-wing flight. One of the advantages of a flapping wing is that it generates lift and thrust without excessive size or weight (see Delaurier & Harris 1982, Kellogg et al. 2001b). In the interest in achieving bird-like or insect-like flight performance, investigators have focused attention on the wing dynamics and unsteady aerodynamics of these creatures. Our understanding of the aerodynamics of bird and insect flight, however, is limited. Birds and insects exploit the coupling between flexible wings and aerodynamic forces (i.e., aeroelasticity) such that the aeroelastic wing deformations improve aerodynamic performance. By flapping their wings, birds and insects effectively increase the Reynolds number seen by the wings without increasing their forward flight speed.

The Harris/DeLaurier radio-controlled ornithopter was developed as a concept vehicle (DeLaurier & Harris 1993). The airfoil used, the S1020, was designed by Selig to have a wide range of angles of attack for attached flow. It is powered by a reciprocating engine and has flown at 54 km/h (34 mph) for approximately 3 min with a flapping frequency of ∼3 Hz. It has a payload capacity of approximately 227 g (8 oz). Details of the unsteady aerodynamics of this vehicle are discussed below (see Section 4).

The MicroBat ornithopter is electrically powered, has a total mass of 12 g (0.423 oz), and the throttle, elevator, and rudder are manually controlled. Although the MicroBat has no payload, it has flown at 19 km/h (12 mph) with a flapping frequency of ∼12 Hz for 6 min. The early research that influenced the MicroBat design was presented by Pornsin-Sirirak et al. (2000).

## 3. AERODYNAMICS OF FIXED-WING VEHICLES

The airfoil section and wing planform of the lifting surface are critically important to the performance of all flying vehicles. Therefore, all small UAVs share the ultimate goal of a stable and controllable vehicle with maximum aerodynamic efficiency. The aerodynamic efficiency is determined by the lift to drag ratio of the wing. Most small vehicles are designed for maximum range or endurance at a given cruising speed (Anderson 2000). For propeller-driven airplanes with reciprocating engines, the maximum range depends on the maximum lift to drag ratio as shown in Brequet's range equation:

$$\text{Range} = \frac{\eta}{c}\frac{C_L}{C_D}\ln\frac{W_0}{W_1}, \tag{1}$$

where $\eta$ is the propeller efficiency, c is the specific fuel consumption, $C_L/C_D$ is the lift to drag ratio, $W_0$ is the gross weight, and $W_1$ is the weight of the airplane without fuel. Thus, the maximum range is directly dependent on the maximum value of $(C_L/C_D)$ at the cruise condition. Brequet's endurance equation for propeller-driven aircraft is

$$\text{Endurance} = \frac{\eta}{c}\frac{C_L^{3/2}}{C_D}(2\rho S)^{1/2}\left(W_1^{-1/2} - W_0^{-1/2}\right), \tag{2}$$

where $\rho$ is the air density and S is the wing area. In order to maximize endurance, one must maximize $(C_L^{3/2}/C_D)$. It should be noted that Equations 1 and 2 do not apply to electrically powered vehicles because their weight remains the same. In this case the goal is to minimize the total power required from the battery for a given flight condition. The endurance is then the battery output power in watt hours divided by the total power required in watts, and the range is the endurance times the cruise velocity. The total drag on the vehicle is

$$C_D = C_{D_0} + \frac{C_L^2}{\pi(AR)e}, \tag{3}$$

where $C_{D_0}$ is the parasite drag coefficient at zero lift and $\frac{C_L^2}{\pi(AR)e}$ includes induced drag due to lift and the contribution to parasite drag due to lift. These equations point to the fact that parasite drag, including skin friction and pressure drag, on all of the vehicle's nonlifting parts must be reduced as much as possible.

In order to reduce $\frac{C_L^2}{\pi(AR)e}$ the aspect ratio (AR), the wingspan squared divided by the projected planform area of the wing, can be increased or the Oswald efficiency factor can be increased. Flying at a moderate lift coefficient will also reduce the induced drag (i.e., the drag due to lift). Because the maximum lift to drag ratio usually occurs at angles of attack where the lift coefficient is somewhat lower than its maximum value, and because the Oswald efficiency factor cannot be easily increased, significant reductions in $\frac{C_L^2}{\pi(AR)e}$ are usually accomplished by increasing the AR.

## 3.1. Boundary-Layer Behavior

It is well known that the performance of airfoils designed for chord Reynolds numbers greater than 500,000 (McMasters & Henderson 1980, Lissaman 1983, Mueller 1985) deteriorates rapidly as the chord Reynolds number decreases below 500,000 because of laminar boundary-layer separation. Furthermore, the performance of three-dimensional wings (i.e., finite wings), as measured by $(C_L/C_D)_{max}$, is less than that for airfoils. Because small UAVs operate in the chord Reynolds number regime ranging from 500,000 down to approximately 30,000, the design of efficient airfoils and wings is critical.

The survey of low Reynolds number airfoils by Carmichael (1981), although two decades old, is a very useful starting point in the description of the character of the flow over airfoils over the range of Reynolds numbers of interest here. The

following discussion of flow regimes ranging from $30{,}000 \leq R \leq 500{,}000$ is a modified version of Carmichael's original work.

- The range $30{,}000 \leq R \leq 70{,}000$ is of great interest to MAV designers as well as model aircraft builders. The choice of an airfoil section is very important in this regime because relatively thick airfoils (i.e., 6% and above) can have significant hysteresis in the lift and drag forces caused by laminar separation with transition to turbulent flow. Below chord Reynolds numbers of ~50,000, the free shear layer after laminar separation normally does not transition to turbulent flow in time to reattach to the airfoil surface. When this separation point reaches the leading edge, the lift decreases abruptly, the drag increases abruptly, and the airfoil is stalled.
- At Reynolds numbers in the range of 70,000 to 200,000, extensive laminar flow can be obtained, and therefore airfoil performance improves unless the laminar separation bubble still presents a problem for a particular airfoil. Many MAVs and small UAVs fly in this range.
- For $R$ above 200,000, airfoil performance improves significantly because the parasite drag due to the separation bubble decreases as the bubbles get shorter. There is a great deal of experience available from large soaring birds, large radio-controlled model airplanes, and human-powered airplanes to support this claim.

## 3.2. Separation Bubble

The postseparation behavior of the laminar boundary layer accounts for the deterioration in airfoil performance at low Reynolds numbers. This deterioration is exhibited in an increase in drag and decrease in lift. In this flow regime, the boundary layer on an airfoil often remains laminar downstream of the minimum pressure and then separates to form a shear layer. At Reynolds numbers below 50,000, this separated shear layer does not reattach. At Reynolds numbers greater than 50,000, transition takes place in the separated shear layer. Provided the adverse pressure gradient is not too large, the flow can recover sufficient energy through entrainment to reattach to the airfoil surface. Thus, on a time-averaged basis, a region of recirculating flow is formed, as shown in Figure 5 (Horton 1968). Because the bubble acts as a boundary-layer trip, the phenomena is often referred to as a transitional separation bubble. At low Reynolds numbers, the transitional bubble can occupy 15%–40% of the airfoil surface and is referred to as a long bubble. The separation bubble often has a dramatic effect on the stalling characteristics (i.e., the drastic decrease in lift and increase in drag) of airfoils. When a short bubble is present, usually at high Reynolds numbers, the lift increases linearly with angle of attack until stall occurs. This is referred to as the bursting of the short bubble. If a long bubble forms on the surface, usually at low Reynolds numbers, stall occurs when it has extended to the trailing edge. The behavior of the separation bubble is also a factor in the occurrence of hysteresis for some airfoils. The

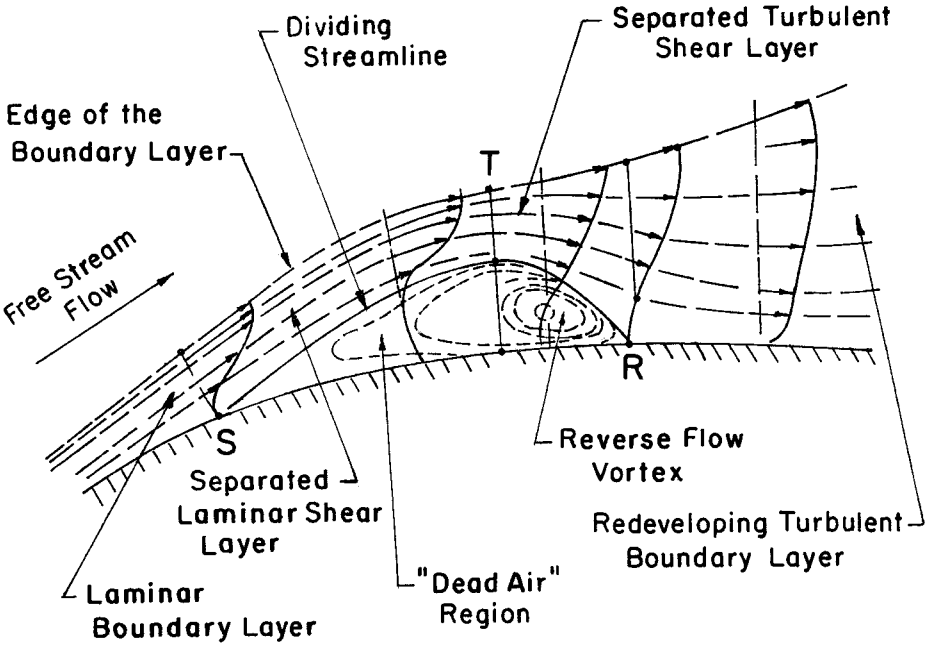


**Figure 5** Time-averaged features of a transitional separation bubble (Horton 1968).

flow is unsteady downstream of the maximum vertical displacement of the bubble. In contrast, flow visualization and hot-wire studies that demonstrate a relatively steady flow upstream of the maximum vertical displacement (*T* in Figure 5) [i.e., where transition to turbulent flow is assumed to take place (Brendel & Mueller 1988a, 1990)] have been conducted. Hence, accurate prediction of the existence and extent of the separation bubble, relative to airfoil performance, is necessary in the design of efficient low-speed airfoils.

## 3.3. High AR Wings

In the early days of small UAV design, one typically did not rely on designing an airfoil section for the particular UAV under consideration. Instead, the designer often used an airfoil section already designed and tested for some other application. For example, the LAURA vehicles shown in Figure 3 used the FX63-137, the RF1165FB, and the LA2573A (Foch & Ailinger 1992). The FX63-137 originally designed by F.X. Wortmann (Althaus & Wortmann 1981) for full-size sailplanes had the highest lift coefficient, 1.4, at cruising speed for the LAURA vehicle, compared to the values of 0.85 for the RF-1165FB (designed by R. Foch of NRL) and 0.68 for the LA2573A (designed by R. Liebeck of Boeing). The FX63-137 was more difficult to fabricate than the other two but had mild stalling characteristics

at Reynolds numbers as low as 100,000. Half-scale models were wind-tunnel tested, and full-scale vehicles were flight tested. The wind-tunnel tests measured maximum lift to drag ratios ranging from ∼20 to 27. The joined-wing vehicle had the lowest value, whereas the variable span had the highest value. Because of its excellent performance in the low Reynolds number regime, this airfoil has been studied extensively. In addition to the studies of lift/drag performance (Althaus 1980, Althaus & Wortmann 1981), investigators have also used the FX63-137 to study the laminar separation bubble on the airfoil (Brendel & Mueller 1988a, Fitzgerald & Mueller 1990), wings with ARs ranging from 3.0 to 5.4 (Bastedo & Mueller 1986), and the influence of unsteady flow on the boundary layer and separation bubble (Brendel & Mueller 1988b, 1990; Ellsworth & Mueller 1991). Using this Wortmann airfoil, Khan & Mueller (1991) conducted other studies on the influence of the tip vortex of a FX63-137 wing on a downstream airfoil with the same geometry, and Scharpf & Mueller (1992) studied the interaction of a closely coupled tandem wing configuration.

Most of the second-generation small UAVs have used airfoil sections designed specifically for their application. The two methods most often used to design airfoils at low Reynolds numbers are attributed to Eppler (1990; Eppler & Somers 1980a,b) and Drela (1989). The latest version of the Eppler code (Richard Eppler Airfoil Program System: Profile 00) may be obtained directly from R. Eppler. The Drela code (XFOIL) may be obtained from the following website: http://raphael.mit.edu/xfoil/. Selig and coworkers (Selig & Maughmer 1992; Selig et al. 1989, 1995, 1996, 2001) have both designed (using the Eppler and Drela codes) and tested a large number of low Reynolds number airfoil sections for sailplanes, radio-controlled model airplanes, and small wind turbines. Some of these airfoils have been successfully used for small UAVs. Catalogs of the Selig airfoils and many other airfoils have been tested for Reynolds number ranging from ∼60,000 to 500,000 (Selig et al. 1989, 1995, 1996; Lyon et al. 1997). This information provides a good starting point in the design process.

## 3.4. Low AR Wings

The aerodynamics of low AR (LAR) wings (i.e., AR below 2.0) at low Reynolds numbers has received very little attention. LAR wings in the form of delta wings have been extensively researched at higher Reynolds numbers at subsonic, transonic, and supersonic speeds. Many of these studies focused on the high angle-of-attack aerodynamics of delta and other types of pointed LAR wings.

Some information is available, however, regarding nondelta LAR wings, with much of the research having been done between the 1930s and the 1950s. Zimmerman (1932, 1935), Bartlett & Vital (1944), and Wadlin et al. (1955) performed experiments using LAR wings at Reynolds numbers greater than 500,000. Theoretical and analytical treatises of LAR wing aerodynamics have been performed by Bollay (1939), Weinig (1947), Bera & Suresh (1989), Polhamus (1966, 1971), and Rajan & Shashidhar (1997). Recently, Pelletier & Mueller (2000) and Mueller

(2000) studied the aerodynamics of rectangular flat and cambered wings with LAR and 2% thickness at Reynolds numbers ranging between 60,000 and 200,000. These wind-tunnel studies also examined the influence of the tunnel freestream turbulence level and trailing-edge shape on performance. Further studies of the effect of camber were reported by Brown (2001).

Perhaps the most complete analysis and review of LAR wings was performed by Hoerner (1965) and Hoerner & Borst (1975) in a two-volume series on lift and drag. Hoerner reviewed many of the theories developed for LAR wings of nondelta planforms. A variety of correlations as well as analytical methods were presented and compared with the available experimental data of the time. Although the information presented by Hoerner corresponds to higher Reynolds numbers than of interest for MAVs, Torres & Mueller (2001) and Torres (2002) have shown that the aerodynamic theory still holds. This theory correctly predicts that as a finite wing of a given AR generates, lift and counter-rotating vortical structures form near the wingtips. These vortices strengthen as the angle of attack increases. For an LAR wing, the tip vortices may be present over most of the wing area and therefore exert great influence on its aerodynamic characteristics. Wings of AR below $\sim$1.5 can be considered to have two sources of lift: linear and nonlinear. The linear lift is created by circulation around the airfoil and is what is typically thought of as lift in higher AR wings. The nonlinear lift is created when the tip vortices form low-pressure cells on the top surface of the wing, as is observed in delta wings at high angles of attack. This nonlinear effect increases the lift-curve slope as the angle of attack increases, and it is considered to be responsible for the high value of stall angle of attack.

## 4. UNSTEADY AERODYNAMICS APPLIED TO OSCILLATING-WING PROPULSION

Originally, virtually all "small flying vehicles" (birds, bats, and insects) had flapping wings. This can be ascribed to Nature working within the constraint of muscle actuation: a biological necessity that need not apply to mechanical flight. Indeed, it was the notion of separating the function of lift from that of propulsion that freed humans from fruitless attempts to imitate animal flight. However, certain noted researchers throughout the years have been intrigued by the challenge of analytically modeling, as well as mechanically implementing, flapping-wing flight. In particular, recent interest in small, low Reynolds number aircraft has motivated researchers to study the possibility that flapping wings may offer some unique aerodynamic advantages at that scale.

### 4.1. Theoretical Studies

The simplest model for flapping-wing aerodynamics assumes quasi-steady behavior where, for each time step during the airfoil's motion, the flow is in an equilibrium condition for the instantaneous boundary conditions. Further, the flow is

fully attached, including around the leading edge (no small-scale localized separation), giving 100% leading-edge suction. Thus, from the Kutta-Joukowski theorem (Kuethe & Chow 1998), the lift vector is always perpendicular to the relative velocity, and one may visualize thrust as being produced by the horizontal component of the lift vector. With this model, Kuechemann & von Holst (1941), in their study of flapping-wing flight, showed that a finite AR wing executing pure plunging motion (no pitching) could achieve a propulsive efficiency, $\eta$, given by

$$\eta = \frac{Thrust \cdot Velocity}{Input\ power} = \frac{1}{1 + 2/AR}, \tag{4}$$

where *AR* is the aspect ratio of the wing. This is of course an idealized result, ignoring flow separation and other viscous effects. However, because the propulsive efficiency approached 100% with increasing AR, this did provide an encouraging baseline case for further exploration of flapping-wing flight.

The quasi-steady model is computationally very straightforward and was extended for conditions involving additional kinematic complexity, such as pitching and plunging as well as root flapping. In particular, this model was utilized by zoologists such as Norberg (1985) and Ellington (1984) in their studies of animal flight. Further, Betteridge & Archer (1974) achieved an especially sophisticated form of the quasi-steady model in their studies of the propulsive efficiency and vertical oscillatory force of a large AR flapping wing. This form was further extended by Jones (1980), who showed the possibility of high efficiencies for optimized spanwise circulation distributions.

The quasi-steady model is only correct for conditions with a very high advance ratio, $\lambda$, which is defined as the number of chord lengths traveled per flapping cycle:

$$\lambda = \frac{Speed}{Chord \cdot Flapping\ frequency} = \frac{U}{cf}. \tag{5}$$

This is, of course, the same argument as for the quasi-steady aerodynamic model used in aircraft flight dynamics. However, this assumption is not justifiable for most flight conditions encountered by animals and ornithopters. Even for fast-cruising flight, the highest advance ratios are on the order of 10, a ratio for which unsteady aerodynamic effects are still significant.

Garrick (1936) performed the first significant analysis on unsteady thrust production with his study of a thin airfoil undergoing plunging and pitching. This was a linearized inviscid-flow solution, building upon the unsteady airfoil analysis by Theodorsen (1935) and the thrust-prediction methodology by von Karman & Burgers (1935). The wake is co-planar with the airfoil, thus limiting the veracity of the solution to fairly high advance ratios. However, the role of leading-edge suction is clearly elucidated, and equations are given for the unsteady leading-edge suction force. Fully attached flow was assumed, so the effect of local leading-edge separation attenuating the suction force was not accounted for. It is a simple matter, however, to assign a leading-edge suction efficiency factor to Garrick's equation (see below).

Propulsive efficiencies were calculated as a function of the inverse of the reduced frequency, 1/k:

$$\frac{1}{k} = \frac{2U}{\omega c} = \frac{1}{\pi}\frac{U}{fc} = \frac{\lambda}{\pi}, \tag{6}$$

where $\omega$ is the oscillation frequency in radians per second and c is the chord. It was found for the pure-plunging airfoil (no pitching) that the propulsive efficiency varied from 50% when the advance ratio equals zero to above 90% when the advance ratio exceeds 45.

The Garrick's oscillating-airfoil model was extended by Fairgrieve & DeLaurier (1982) to account for nonplanar wakes and periodic but nonsinusoidal oscillation. The idea was that motion with unequal times between upstroke and downstroke, or functional shapes differing from pure sinusoidal, may offer some increase in thrust production or propulsive efficiency. However, none of the cases studied offered clear advantages over simple harmonic motion (equal upstroke and downstroke sinusoidal motion). Also, a surprising result was that the planar-wake solutions closely matched those for the frozen wavy wake and time-deforming wake models, down to advance ratios ≈6. A similar result was found by Hall & Hall (2001) for an airfoil with a frozen and a free wake.

The Garrick model was also used in the development of an analysis for an ornithopter wing design (DeLaurier 1993a). The basis of the physical model is that the wing is conceptually divided into segments ("strip theory") upon which normal forces, pitching moments, and chordwise forces, including leading-edge suction, act in response to plunging and pitching motions (Figure 6). Camber and mean angle of attack are included, as well as apparent-mass effects and partial leading-edge suction (defined by a leading-edge suction efficiency parameter). Further, the unsteady shed vortex wake is accounted for by using the finite-wing

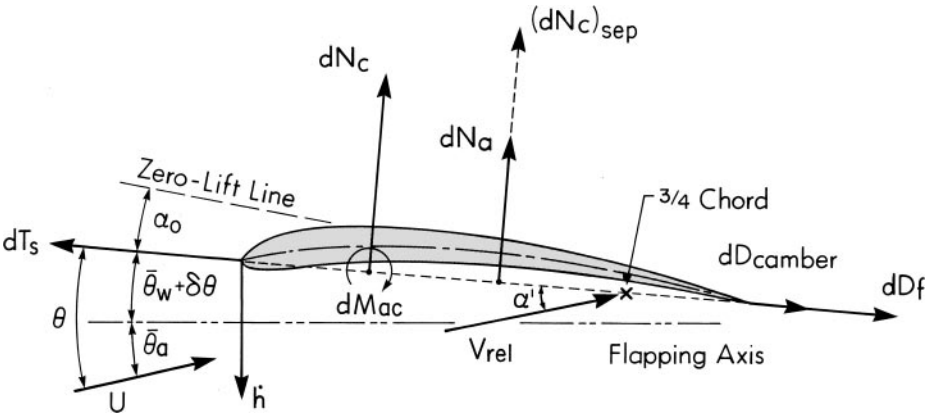


**Figure 6** Wing-section aerodynamic forces and motion variables.

extension of the Theodorsen unsteady-airfoil model by Jones (1940). This requires the assumption that every segment of the flapping wing acts as if it were part of a wing of the same AR, executing whole-wing plunging and pitching equal to that of the segment.

Another feature is that the individual segments are allowed to stall during the flapping cycle in accordance to the dynamic-stall criteria by Prouty (1986). However, it is clear that this modified strip-theory approach involves significant assumptions. For instance, portions of wings rarely stall without affecting the loading on the rest of the wing. The same observation may be made regarding the incorporation of the unsteady-wake model. However, this analysis was motivated by an ornithopter development project that required a straightforward and readily implemented design tool. As a result, subsequent wind-tunnel testing showed wing performance matching closely with predictions. Furthermore, this analysis was evaluated by Winfield (1990) in comparison with an unsteady marching-vortex model, and very favorable results were obtained, as seen in Figure 7.

The analysis was further extended by incorporating it into a structural-deformation program, so that the wing's twisting and bending (Figure 8) in response to the imposed flapping could be predicted (DeLaurier 1993b). Therefore, one may specify the geometric, inertial, elastic, and aerodynamic parameters of the sections along the span and then predict the lift, thrust, and bending moments as well as the required flapping moment and input power. This allowed a design iteration to be performed, converging to a wing that produced successful flight (Delaurier & Harris 1993).

The flapping wings, as incorporated into the ornithopter, are hinged to a rigid center wing that performs plunging motions only as required by the design for actuating the wings (Figure 9*a*). Also, this feature serves to balance the unsteady

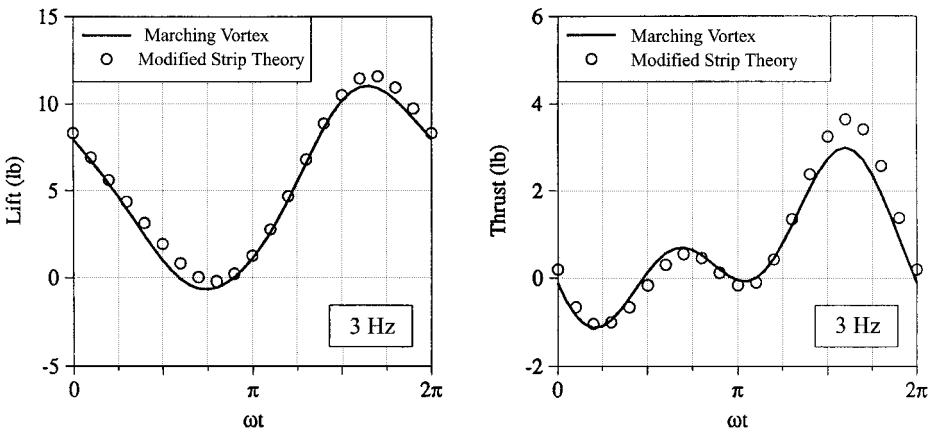


**Figure 7** Comparison of marching-vortex and strip-theory results.

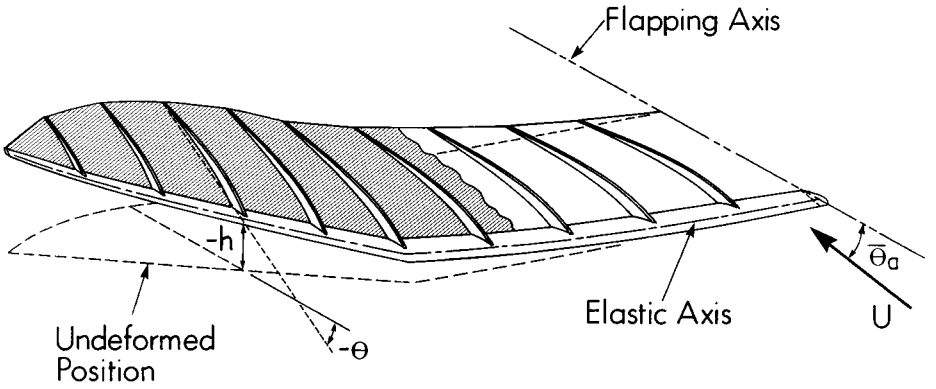


**Figure 8** Wing structural-deformation model.



vertical acceleration transmitted to the fuselage. The analysis was extended to account for the center wing (DeLaurier 1994), in which case the performance characteristics of the entire wing could be assessed. It was determined that the propulsive efficiency was 54%, which does not seem very high until one realizes that this also accounts for the energy loss from the wing's induced drag. When this is subtracted, which makes the resulting value more fairly comparable to the definition of propeller efficiency, the propulsive efficiency was 79%. This is a reasonable value for the scale of the model, and it would become higher as an ornithopter's size increased because the leading-edge suction efficiency approaches 100% at larger Reynolds numbers. In fact, it should be emphasized that the primary thrust force for this wing comes from leading-edge suction. An airfoil of 15% thickness (S1020) was especially designed for this application by M. Selig of the University of Illinois, and the main purpose of twisting is to reduce the relative angles of attack below stall values during the flapping cycle. This contrasts with the airfoils of birds and bats, which are thin cambered sections with relatively sharp leading edges and very low leading-edge suction efficiency. In that case, twisting is required in order to give a horizontal component to the normal-force vector for thrust production.

## 4.2. Experimental Studies

Obtaining good experimental data for oscillating and flapping wings is a considerable challenge because the inertial-reaction forces can often obscure the relatively small thrust forces being measured. Therefore, the body of literature on this is much smaller than that for the theoretical studies. Archer et al. (1979) performed experiments on a root-flapping elastic wing in a wind tunnel and obtained values for thrust and propulsive efficiency that reasonably matched predictions from their quasi-steady analysis. However, it was not possible to obtain sufficient data to confirm all of the theoretical trends.

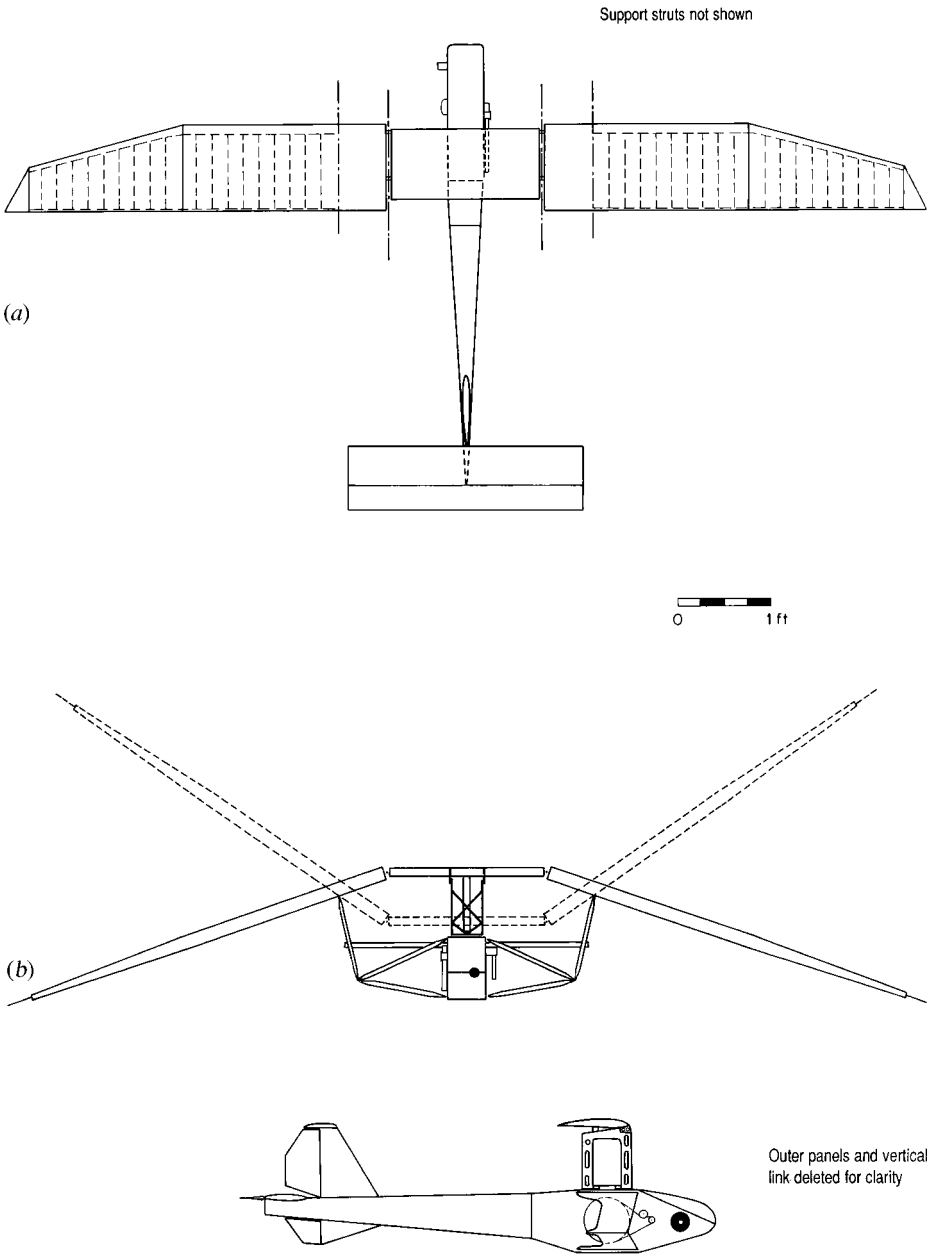


**Figure 9** (*a*) Top view of a Harris/DeLaurier ornithopter. (*b*) Side and front views of a Harris/DeLaurier ornithopter.

Experiments were also conducted by Fejtek & Nehera (1980) on a root-flapping rigid wing with a thick cambered airfoil. Although this could be set at various incidence angles, there was no pitch articulation during the flapping cycle. Instantaneous thrust and lift values, but not propulsive efficiency, were measured, yet no positive thrusts were achieved, which was probably owing to flow separation during the flapping cycle (pitching at certain phase angles and amplitudes could have served to suppress this). A comparison was made with quasi-steady theoretical models, but the matching was inconclusive.

Wind-tunnel tests were conducted by DeLaurier & Harris (1982) on a rigid wing with an AR of 4.0 and an NACA 0012 airfoil subjected to uniform sinusoidal plunging, $h$, and pitching, $\theta$:

$$h = h_0 \sin \omega t \qquad \theta = \theta_0 \sin(\omega t + \delta), \tag{7}$$

where $h_0 = 0.625c$; $\theta_0 = 0.0, 5.7^\circ, 8.4^\circ, 12.1^\circ$; and $\delta = 60^\circ, 75^\circ, 90^\circ, 105^\circ, 120^\circ$. The reduced frequency, $k$, varied from 0.045 to 0.16 for the case where $\theta_0 = 0.0$, and 0.07 to 0.16 for all other cases. The average thrust coefficients, $\bar{C}_T$, were obtained based on

$$\bar{C}_T = \frac{\textit{Average thrust}}{\left[(\rho/2)\, U^2 S\, (2h_{\max}/c)^2\right]}, \tag{8}$$

where $h_{\max}$ is the maximum vertical excursion of any point on the airfoil. The $\bar{C}_T$ values varied almost linearly with $k$, and the largest values of $\bar{C}_T (\approx 0.023)$ were achieved with $\theta_0 = 12.1^\circ$ and phase angles, $\delta$, ranging between $60^\circ$ and $90^\circ$. Limitations of the equipment, however, prevented measurement of the propulsive efficiencies.

Experiments were also conducted on candidate wings for the ornithopter mentioned previously (DeLaurier 1993b). In this case, the wings were attached to a wire-suspended platform mounted above the ceiling of the test section. The platform carried the electric-motor drive to flap the wing, and the suspension allowed free movement parallel to the ceiling, which was constrained by strain gages calibrated to measure the thrust, lift, and pitching moment of the wing.

The most successful wing was the Mark-8 design, shown in Figure 9*b* as incorporated into the ornithopter. The wind-tunnel results for this are shown in Figure 10 (compared with the predictions from the analysis). The average thrust values match closely. However, the lift values are somewhat overpredicted, which could be owing to imperfect reflecting-plane effects at the wing's root. What does match is the interesting result that the average lift stays essentially constant with flapping frequency. This has important consequences for the way in which an ornithopter is trimmed for stable flight. Namely, for this type of wing, the criteria for tail volume and static margin may be drawn from fixed-wing aircraft practice.

Flight tests confirmed the wind-tunnel results in that the wing design successfully sustained the ornithopter (Figure 11). Also, the aircraft was very stable and readily controlled. Overall, the flight performance closely matched the predictions.

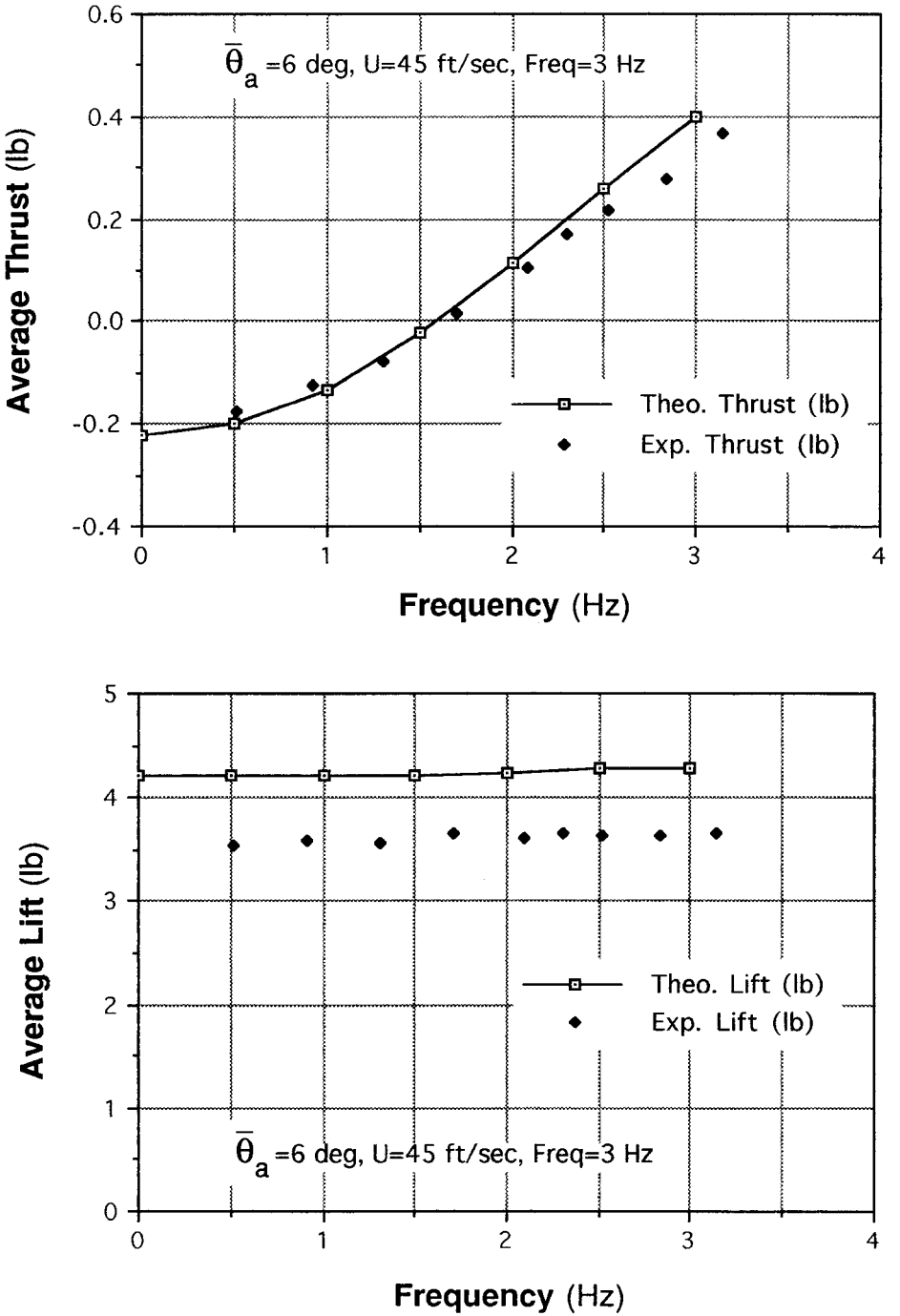


**Figure 10** Ornithopter wing performance.

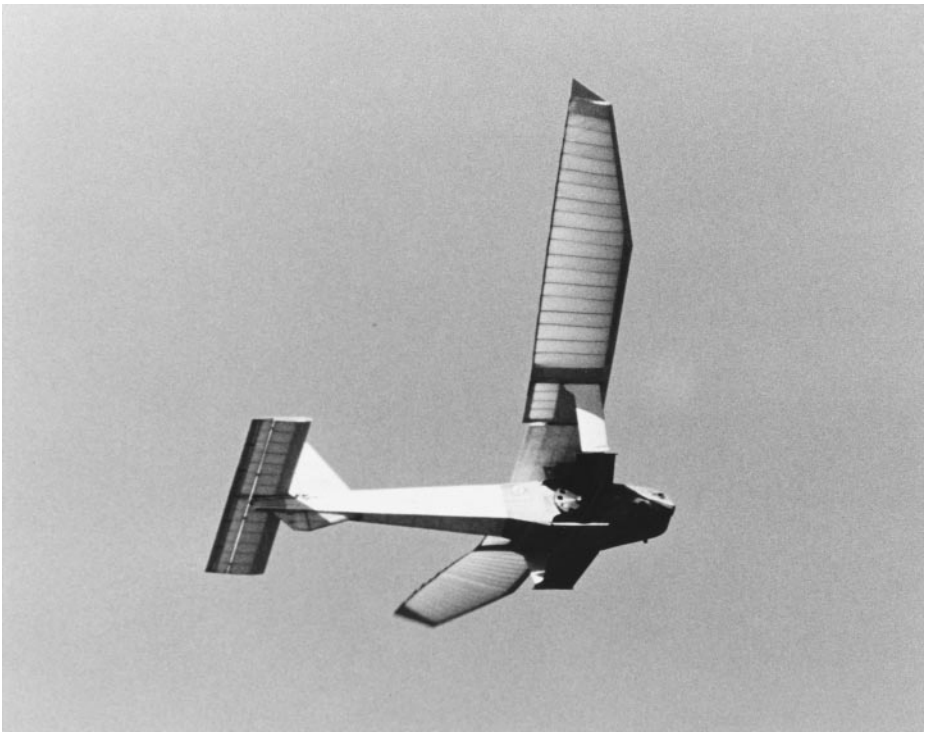

**Figure 11** Ornithopter in flight.

## 5. CONCLUDING REMARKS

The aerodynamics of fixed-wing vehicles is critically dependent on the Reynolds number and AR of the wing. Existing airfoil design methods produce good results down to Reynolds numbers of 200,000. These airfoil design methods pay particular attention to the management of the airfoil boundary layer so as to reduce the adverse effects of laminar separation bubbles. When the AR decreases below 1.5, the nonlinear lift from the tip vortices dominates, especially at high angles of attack. For this reason, MAVs tend to cruise at higher angles of attack than higher AR vehicles. The small fixed-wing UAVs and MAVs described here indicate that there is sufficient experience to design vehicles with good performance.

The design-oriented analysis for flapping wings is applicable to defining the wing configuration for a successful ornithopter. However, it should be noted that considerable refinement is possible if the strip-theory limitation can be overcome while retaining the local flow-separation feature. Also, the theory was specialized for a vehicle in translational flight at advance ratios high enough so that a planar wake and a mostly attached flow can be assumed. These assumptions do not

apply for very slow speed or hovering flight, where the vortex wake is nonplanar and shed leading-edge vortices have an important influence on the propulsive and lifting efficiencies. These are topics of considerable current interest for application to MAVs. Indeed, to take the history of flight back to its origins, the fundamental notion is that biomimetics may hold the key to extraordinary performance at the micro scale.



## ACKNOWLEDGMENTS

The authors would like to thank A. Cross, R. Foch, and J. Kellogg of the U.S. Naval Research Laboratory; J. Grasmeyer of AeroVironment, Inc.; and P. Ifju and W. Shyy of the University of Florida for their help in the preparation of this manuscript. We would also like to acknowledge the support of the Natural Science and Engineering Research Council of Canada.

**The *Annual Review of Fluid Mechanics* is online at http://fluid.annualreviews.org**

## LITERATURE CITED

Anderson JD. 2000. *Introduction to Flight*. Boston: McGraw-Hill. 766 pp.

Althaus D. 1980. *Profilpolaren fuer den Modellflug*. Germany: CF Mueller. 176 pp.

Althaus D, Wortmann FX. 1981. *Stuttgarter Profilkatalog I.* Braunschweig, Ger.: E Hunold

Archer RD, Sapuppo J, Betteridge DS. 1979. Propulsion characteristics of flapping wings. *Aeronaut. J.* 83:355–71

Bartlett GE, Vidal RJ. 1944. Experimental investigation of influence of edge shape on the aerodynamic characteristics of low aspect ratio wings at low speed. *J. Aeronaut. Sci.* 22:517–33

Bastedo WG Jr, Mueller TJ. 1986. The spanwise variation of laminar separation bubbles on finite wings at low Reynolds numbers. *AIAA J. Flight* 23:687–94

Bera RK, Suresh G. 1989. Comments on the Lawrence equation for low-aspect-ratio wings. *J. Aircr.* 26:883–85

Betteridge DS, Archer RD. 1974. A study of the mechanics of flapping wings. *Aeronaut. Q.* 25:129–42

Bollay W. 1939. A non-linear wing-theory and its application to rectangular wings of small aspect ratio. *Z. Angew. Math. Mech.* 19:21–35

Brendel M, Mueller TJ. 1988a. Boundary layer measurements on an airfoil at low Reynolds numbers. *AIAA J. Aircr.* 25:612–17

Brendel M, Mueller TJ. 1988b. Boundary layer measurements on an airfoil at a low Reynolds number in an oscillating freestream. *AIAA J.* 26:257–63

Brendel M, Mueller TJ. 1990. Transition phenomenon on airfoils operating at low chord Reynolds numbers in steady and unsteady flows. In *Numerical and Physical Aspects of Aerodynamic Flows IV*, ed. T Cebeci, pp. 333–44. Berlin: Springer-Verlag

Broeren AP, Bragg MB. 2001. Unsteady stalling characteristics of thin airfoils at low Reynolds number. In *Fixed and Flapping Wing Aerodynamics for Micro Air Vehicle Applications*, ed. TJ Mueller, 195:191–213. Reston, VA: AIAA. 586 pp.

Brown CA. 2001. *The effect of camber on thin plate low aspect ratio wings at low Reynolds numbers.* MS thesis. Univ. Notre Dame, Notre Dame, IN

Carmichael BH. 1981. Low Reynolds number airfoil survey. Vol. 1. *NASA CR 165803*

Cross A. 1989. Captive carry testing of remotely piloted vehicles. In *Low Reynolds Number Aerodynamics*, ed. TJ Mueller, 54:394–406. Germany: Springer-Verlag. 446 pp.

DeLaurier JD. 1993a. An aerodynamic model for flapping-wing flight. *Aeronaut. J.* 97: 125–30

DeLaurier JD. 1993b. The development of an efficient ornithopter wing. *Aeronaut. J.* 97: 153–62

DeLaurier JD. 1994. An ornithopter wing design. *Can. Aeronaut. Space J.* 40:10–18

DeLaurier JD, Harris JM. 1982. Experimental study of oscillating-wing propulsion. *J. Aircr.* 19:368–73

DeLaurier JD, Harris JM. 1993. A study of mechanical flapping wing flight. *Aeronaut. J.* 97:277–86

Drela M. 1989. An analysis and design system for low Reynolds number airfoils. See Cross 1989, pp. 1–12

Ellington CP. 1984. The aerodynamics of hovering insect flight. I. The quasi-steady analysis. *Philos. Trans. R. Soc. London Ser. A* 305:1–15

Ellsworth RH, Mueller TJ. 1991. Airfoil boundary layer measurements at low *Re* in an accelerating flow from a nonzero velocity. *Exp. Fluids* 11:368–74

Eppler R. 1990. *Airfoil Design and Data*. Berlin: Springer-Verlag. 562 pp.

Eppler R, Somers DM. 1980a. A computer program for the design and analysis of low-speed airfoils. *NASA-TM-80210*

Eppler R, Somers DM. 1980b. A computer program for the design and analysis of low-speed airfoils. Suppl. *NASA-TM-80210*

Evangelista R, McGhee RJ, Walker BS. 1989. Correlation of theory to wind-tunnel data at Reynolds numbers below 500,000. See Cross 1989, pp. 146–60

Fairgrieve JD, DeLaurier JD. 1982. Propulsive performance of two-dimensional thin airfoils undergoing large-amplitude pitch and plunge oscillations. *Univ. of Toronto Inst. Aerosp. Studies. Tech. Note 226*

Fejtek I, Nehara J. 1980. Experimental study of flapping wing lift and propulsion. *Aeronaut. J.* 84:28–33

Fitzgerald EJ, Mueller TJ. 1990. Measurements in a separation bubble on an airfoil using laser velocimetry. *AIAA J.* 28:584–92

Foch RJ. 1996. A low cost airobotic platform. *Proc. AUVSI, Florida*, pp. 863–68. Arlington, VA: Assoc. Unmanned Veh. Syst. Int.

Foch RJ, Dahlburg JP, McMains JW, Bovais CS, Carruthers SL, et al. 2000. Dragon Eye, an airborne sensor system for small units. *Proc. Unmanned Systems, Florida*, pp 1–13. St. Louis, MO: Mira CD-Rom Publ.

Foch RJ, Ailinger KG. 1992. *Low Reynolds number, long endurance aircraft design.* AIAA 92–1263. Presented at Aerosp. Design Conf., AIAA, Irvine, CA

Foch RJ, Toot PL. 1989. Flight testing Navy low Reynolds number (LRN) unmanned aircraft. See Cross 1989, pp. 407–17

Garrick IE. 1936. Propulsion of a flapping and oscillating airfoil. *NACA Tech. Rep. 567*

Grasmeyer JM, Keennon MT. 2001. Development of the Black Widow micro-air vehicle. See Broeren and Bragg 2001, pp. 519–35

Hall KC, Hall SR. 2001. A rational engineering analysis of the efficiency of flapping flight. In *Fixed and Flapping Wing Aerodynamics for Micro Air Vehicle Applications, Progress in Aeronautics and Astronautics*, ed. TJ Mueller, pp. 249–74. Reston, VA: AIAA

Hoerner SF. 1965. *Fluid-Dynamic Drag.* Brick Town, NJ: Hoerner Fluid Mech.

Hoerner SF, Borst HV. 1975. *Fluid-Dynamic Lift.* Brick Town, NJ: Hoerner Fluid Mech.

Horton HP. 1968. *Laminar separation bubbles in two and three-dimensional incompressible flow*. PhD thesis. Univ. London, UK

Ifju PG, Jenkins DA, Ettinger S, Lian Y, Shyy W, et al. 2002. Flexible-wing-based micro air vehicles. *AIAA Aerosp. Sci. Meet. Exhibit, 40th, Reno*, pp. 1–13. AIAA 2002-0705. Virginia: AIAA

Jones RT. 1940. The unsteady lift of a wing of finite aspect ratio. *NACA Tech. Rep. 681*

Jones RT. 1980. Wing flapping with minimum energy. *NASA TMJ 81174*

Khan FA, Mueller TJ. 1991. Tip vortex/airfoil interaction for a low Reynolds number canard/wing configuration. *AIAA J. Aircr.* 28: 181–86

Kellogg J, Bovais C, Dahlburg J, Foch R, Gardner J, et al. 2001a. The NRL Mite air vehicle. *Proc. Int. Conf. Unmanned Air Veh. Syst., 16th, Bristol, UK*, pp. 25.1–14. Bristol, UK: Univ. Bristol

Kellogg J, Bovais C, Cylinder D, Dahlburg J, Foch R, et al. 2001b. Non-conventional aerodynamics for MAVs. *Proc. Int. Conf. Unmanned Air Veh. Syst., 16th, Bristol, UK*, pp. 26.1–12. Bristol, UK: Univ. Bristol

Kuechemann D, von Holst E. 1941. Aerodynamics of animal flight. *Luftwissen* 9:277–82

Kuethe AM, Chow C-Y. 1998. Irrotational incompressible flow about two-dimensional bodies. In *Foundations of Aerodynamics*, pp. 104–7. New York. Wiley & Sons

Levin O, Shyy W. 2001. Optimization of a low Reynolds number airfoil with flexible membrane. *Comput. Model. Eng. Sci.* 2:523–36

Lissaman PBS. 1983. Low-Reynolds-number airfoils. *Annu. Rev. Fluid Mech.* 15:223–39

Lyon CA, Broeren AP, Giguere P, Gopalarathnam A, Selig MS. 1997. *Summary of Low-Speed Airfoil Data*, Vol. 3. Virginia Beach: SoarTech Publ. 417 pp.

McMasters JH, Henderson ML. 1980. Low-speed single-element airfoil synthesis. *Tech. Soar.* 6:1–21

Mueller TJ. 1985. Low Reynolds number vehicles. In *Advisory Group for Aerospace Research and Development AGARD-AG-288*, ed. E Reshotko. Essex: Spec. Print. Serv. Ltd. 69 pp.

Mueller TJ. 2000. Aerodynamic measurements at low Reynolds numbers for fixed wing micro-air vehicles. In *Development and Operation of UAVs for Military and Civil Applications*. Quebec: Can. Commun. Group Inc. 302 pp.

Norberg UM. 1985. Evolution of vertebrate flight: an aerodynamic model for the transition from gliding to active flight. *Am. Nat.* 126:303–27

Pelletier A, Mueller TJ. 2000. Low Reynolds number aerodynamics of low-aspect-ratio, thin/flat/cambered plate wings. *J. Aircr.* 37: 825–32

Polhamus EC. 1966. A concept of the vortex lift of sharp-edge delta wings based on a leading-edge-suction analogy. *NASA Tech. Rep. TN D-3767*

Polhamus EC. 1971. Predictions of vortex-lift characteristics by a leading-edge-suction analogy. *J. Aircr.* 8:193–99

Pornsin-Sirirak TN, Lee SW, Nassef H, Grasmeyer J, Tai YC, et al. 2000. *MEMS wing technology for a battery-powered ornithopter.* Presented at Int. Conf. Micro Electro Mech. Syst., IEEE, 18th, Miyazaki, Japan

Prouty RW. 1986. Airfoils for rotor blades. In *Helicopter Performance, Stability, and Control*, pp. 397–409. Boston: PWS Eng.

Rajan SC, Shashidhar S. 1997. Exact leading-term solution for low aspect ratio wings. *J. Aircr.* 34:571–73

Scharpf DF, Mueller TJ. 1992. Experimental study of a low Reynolds number tandem airfoil configuration. *AIAA J. Aircr.* 29:231–36

Selig MS, Donovan JF, Fraser DB. 1989. *Airfoils at Low Speeds*, pp. 62–63, 149. Virginia Beach: HA Stokely. 398 pp.

Selig MS, Gopalarathnam A, Giguere P, Lyon CA. 2001. Systematic airfoil design studies at low Reynolds numbers. See Broeren & Bragg 2001, pp. 143–67

Selig MS, Guglielmo JJ, Broeren AP, Giguere P. 1995. *Summary of Low-Speed Airfoil Data,* Vol. 1. Virginia Beach: SoarTech Publ. 292 pp.

Selig MS, Lyon CA, Giguere P, Ninham CP, Guglielmo JJ. 1996. *Summary of Low-Speed Airfoil Data*, Vol. 2. Virginia Beach: SoarTech Publ. 252 pp.

Selig MS, Maughmer MD. 1992. Generalized multipoint inverse airfoil design. *AIAA J.* 30: 2618–25

Shyy W, Berg M, Ljungqvist D. 1999. Flapping and flexible wings for biological and

micro air vehicles. *Progr. Aerosp. Sci.* 35: 455–505

Siddiqi S, Evangelista R, Kwa TS. 1989. The design of a low Reynolds number RPV. See Cross 1989, pp. 381–93

Theodorsen T. 1935. General theory of aerodynamic instability and the mechanism of flutter. *NACA Tech. Rep. 496*

Torres GE, Mueller TJ. 2001. Aerodynamic characteristics of low aspect ratio wings at low Reynolds numbers. See Broeren & Bragg 2001, pp.115–41

Torres GE. 2002. *Aerodynamics of low aspect ratio wings at low Reynolds numbers with applications to micro air vehicle design and optimization.* PhD thesis. Univ. Notre Dame, Notre Dame, IN. 250 pp.

von Karman T, Burgers JM. 1935. Problems of non-uniform and of curvilinear motion. In *Aerodynamic Theory: A General Review of Progress. Vol. II: General Aerodynamic Theory, Perfect Fluids*, ed. WF Durand, pp. 304–10. Berlin: Julius Springer

Wadlin KL, Ramsen JA, Vaughan VL Jr. 1955. The hydrodynamic characteristics of modified rectangular flat plates having aspect ratios of 1.00, 0.25, and 0.125 and operating near a free water surface. *NACA Tech. Rep. TR 1246*

Weinig F. 1947. Lift and drag of wings with small span. *NACA Tech. Rep. TM-1151*

Winfield, JF. 1990. *A three-dimensional unsteady aerodynamic model with applications to flapping-wing propulsion.* MA thesis. Univ. Toronto Inst. Aerosp. Stud., Toronto. 180 pp.

Zimmerman CH. 1932 . Characteristics of Clark Y airfoils of small aspect ratios. *NACA Tech. Rep. TR 431*

Zimmerman CH. 1935. Characteristics of several airfoils of low aspect ratio. *NACA Tech. Note 539*

*Annual Review of Fluid Mechanics*
*Volume 35, 2003*

# CONTENTS